Analysis of an Enzyme–Substrate Complex by X-ray Crystallography and Transferred Nuclear Overhauser Enhancement Measurements: Porcine Pancreatic Elastase and a Hexapeptide[†]

Edgar F. Meyer, Jr.,*,[‡] G. Marius Clore,*,[§] Angela M. Gronenborn,[§] and Harly A. S. Hansen[‡]

Department of Biochemistry and Biophysics, Texas A&M University, College Station, Texas 77843-2128, and Max-Planck-Institut für Biochemie, D-8033 Martinsried bei München, FRG

Received June 24, 1987; Revised Manuscript Received September 4, 1987

ABSTRACT: The hexapeptide substrate Thr-Pro-nVal-NMeLeu-Tyr-Thr reacts with porcine pancreatic elastase sufficiently slowly that accelerated crystallographic data collection procedures and two-dimensional transferred nuclear Overhauser enhancement measurements could be used to study the geometry of binding. Both studies report a time-averaged population of the Michaelis complex state, prior to proteolysis. This result provides an important data point along the reaction coordinate pathway for serine proteases. Crystallographic data to 1.80-Å resolution were used in the structure analysis with refinement to an *R*-factor of 0.19.

With the exception of inhibited complexes, most enzymatic reactions are opaque to investigation of structure–functional relationships in and around the active site. A number of details about the reaction mechanism of the serine proteases therefore remain poorly understood. In this paper we describe two complementary experiments designed to probe structural details of a kinetically retarded reaction involving porcine pancreatic elastase (PPE).[1]

On the basis of molecular orbital considerations proposed by Deslongchamps (1975), Bizzozero and Zweifel (1975) showed that α-chymotrypsin does not cleave a peptide (or ester) bond when the "leaving-group" N (or C) atom is alkylated (Pro or sarcosine). Bizzozero and Dutler (1981) extended this study to suggest that a stereochemical inversion is the committing step in proteolysis; a methylated peptide-bond N atom is thereby restrained from rapid inversion. The slow turnover of the reaction described here supports these hypotheses and provides a means to view structural interactions within a functioning enzyme.

Our first attempt to test this hypothesis with PPE using as a substrate Pro-Ala-Pro-Tyr led to backward, nonproductive binding (Clore et al., 1986a). We therefore chose to study a hexapeptide, Thr-Pro-nVal-NMeLeu-Tyr-Thr, designed to bind unambiguously to porcine pancreatic elastase. As before (Clore et al., 1986a), a dual-pronged attack, using both high-resolution crystallography and NMR spectroscopy involving the use of TRNOE measurements (Clore & Gronenborn, 1982, 1983), was initiated. Because of the lability of the complex, the crystallographic data collection was limited by a regimen chosen to ensure adequate ligand binding: 24 h of soaking and 48 h of data collection. Such a regimen places a severe strain on conventional crystallographic measurements, which traditionally can require weeks to months to complete. Similarly, the NMR measurements were limited to 24 h of data collection per sample.

EXPERIMENTAL PROCEDURES

Samples. PPE was purchased from Serva (20931) and used without further purification. The hexapeptide Thr-Pro-nVal-NMeLeu-Tyr-Thr was synthesized by Bachem (Switz-erland) and was >99.5% pure as judged by HPLC.

Crystallography. Crystals of PPE were grown from a 0.1 M phosphate buffer (pH 5.0) (Meyer et al., 1986) and harvested with a 0.1 M sulfate plus 0.1 M phosphate (pH 5.0) buffer. A crystal (0.4 × 0.6 × 0.6 mm) was mounted in a thin-walled capillary (0.7-mm diameter) that contained several loops of virgin wool. Several additional loops of virgin wool were then inserted and used as gentle clamps to fix the position of the crystal, which was surrounded by ca. 30 μL of the above buffer solution.

A 0.4-mg sample of hexapeptide was introduced to the crystal in the capillary. Several cracks appeared in the crystal under the polarizing microscope, but they did not appear to be serious, as borne out by the diffraction diagrams. After a 24-h soaking at 19 °C, the crystal was mounted along the needle (*b*) axis on a goniometer head with a deliberate missetting of the vertical and horizontal arcs of +3.5° and +9°. Rotation photographs were taken with a range of 3° and a rotation rate of 1°/h (or multiples thereof) on a 60-mm Huber camera with a crystal-to-film distance of 49 mm. The temperature was 19 ± 1 °C. Data were measured over a spindle axis rotation range of 31.5°, omitting alternating 3° ranges for the sake of accelerating data collection [method of Radhakrishnan et al. (1987)] for 48 h. A Rigaku-Denki rotating anode generator (Cu monochromatized radiation) was operated at 40 kV and 90 mA; a 0.5-mm collimator was used.

A second crystal of similar size was soaked in 0.5 mg of hexapeptide for 24 h. The crystal was misaligned on the goniometer head along the *b* axis with vertical and horizontal arc missetting angles of −9.9° and −2.5°. Data were measured, as with the previous procedure, over a rotation range of 41° over 48 h. Further data were discarded because a precipitate was discovered after microscopic observation; this was taken as an indication of advanced substrate cleavage and hence an indication of potential depletion of substrate and receptor site occupancy.

A third crystal, 0.2 × 0.5 × 1.3 mm, was mounted along the *b* axis as above with missetting angles of 14.9° and 4.1° and reacted with 0.5 mg of hexapeptide substrate for a 24-h

---

[1] Abbreviations: PPE, porcine pancreatic elastase (EC 3.4.21.11); NOE, nuclear Overhauser effect; TRNOE, transferred NOE; NOESY, two-dimensional NOE spectroscopy; HOHAHA, homonuclear Hartmann–Hahn spectroscopy; EDTA, ethylenediaminetetraacetate; nVal, norvaline; NMeLeu, *N*-methylleucine.

Table I: Data Collection and Refinement Statistics

	crystal no.		
	1	2	3
size (mm)	0.4 × 0.6 × 0.6	0.4 × 0.4 × 0.6	0.2 × 0.5 × 1.3
cell axis (Å)	$a = 50.81$	$a = 50.93$	$a = 50.66$
	$b = 58.11$	$b = 58.19$	$b = 58.12$
	$c = 75.50$	$c = 75.53$	$c = 74.96$
temp (°C)	19	19	0

space group	$P2_12_12_1$	effective resolution range[a] (Å)	2.25
no. of atoms/asymmetric unit	2024	SD of 1964 bond lengths (Å)	0.020
		SD of 2716 bond angles (deg)	2.98
overall temp facto ($Å^2$)	16.0	features of final residual density map ($e/Å^3$)	
R-factor ($R = \sum \lVert F_o\rvert - \lvert F_c\rVert / \sum\lvert F_o\rvert$)	0.19	max height	0.42
		min height	−0.42
		SD	0.092
no. of reflections	16543		
data resolution (Å)	1.7		

[a] As defined by Swanson (1987).

soaking period at 0 °C. The goniometer was placed on a Nonius precession camera modified (Huber) for oscillation photography with a crystal to film distance of 49.8 mm. A sealed tube generator at 40 kV, 35 mA (Cu) was used with a monochromator and a 0.5-mm collimator. The measurements were made at 0 ± 0.5 °C for 48 h with a rotation rate generally of 300 min/3° (or an integral multiple thereof) over a spindl. axis range of 32°. After 48 h, while the crystal was kept at 0 °C, an additional 0.2 mg of substrate was added. An additional 9° rotation range was photographed. The crystal was then mounted along the c axis and photographed over a range of 21°, as above; missetting angles were −13.7° and −2.8°. Cell dimensions (Table I) do not vary greatly as a function of temperature in 0.1 M phosphate buffer.

A total of 36 319 reflections (above the 1σ level) was evaluated by using the program FILME (Schwager et al., 1975, with modifications by William Bennett, unpublished data) and loaded into the PROTEIN system (Steigemann, 1974). A total of 16 543 unique reflections was scaled and merged. RSYMM measures the agreement of multiple measurements within a film pack; values ranged from 0.037 to 0.092. RSCALE measures, for each film pack, the agreement of the mean values of reflections derived from at least two sources; values ranged from 0.086 to 0.153 with a mean value of 0.109. The completeness ratio (3.16–1.80-Å resolution) was 74.6%; the last data shell (1.83–1.80-Å resolution) was 43.4% complete. The effective resolution of this data set (Swanson, 1987) is 2.25 Å.

This somewhat elaborate experimental section was necessary because very little prior knowledge was available about the turnover rate of the receptor–substrate complex as a function of buffer, pH, and temperature. To ensure high occupancy of the receptor site, a conservative approach was taken in trying to measure data before obvious precipitation occurred. No corrections for absorption were made. Crystal decay is known not to play a role when exposure times are less than ca. 1 week.

Isomorphous atomic coordinates of PPE were used to phase a difference Fourier map ($R = 0.23$). A model of the hexapeptide was fitted into the residual density and refined with the EREF (Jack & Levitt, 1978; Deisenhofer et al., 1986) set of programs. After approximately 50 successive cycles of refinement of positional coordinates and isotropic temperature factors, the R-factor converged at 0.19 ($R = \sum\lVert F_o\rvert - \lvert F_c\rVert / \sum\lvert F_o\rvert$). The positions of one sulfate, one calcium ion, and 145 bound water molecules were revealed in difference Fourier maps during the refinement.

Table II: Proton Resonance Assignments of the Free Hexapeptide at 5 °C[a]

	chemical shift[b] (ppm)			
residue	NH	$C^\alpha H$	$C^\beta H$	others
Thr-1		4.23	4.23	$C^\gamma H_3$ 1.37
Pro-2		4.53	2.30, 1.83	$C^\gamma H$ 2.02, 1.99; $C^\delta H$ 3.81, 3.67
nVal-3	8.37	4.62	1.60, 1.47	$C^\gamma H$ 1.47, 1.34; $C^\delta H_3$ 0.92
NMeLeu-4		5.06	1.61, 1.52	NCH_3 2.81; $C^\gamma H$ 1.32; $C^\delta H_3$ 0.89, 0.80
Tyr-5	7.87	4.75	3.22, 2.90	$C^\delta H$ 6.81; $C^\epsilon H$ 7.19
Thr-6	8.08	4.34	4.34	$C^\gamma H_3$ 1.17

[a] The resonance positions of the free hexapeptide were assigned by using two-dimensional MLEV17 HOHAHA spectroscopy (Davis & Bax, 1985; Bax & Davis, 1985) in both D_2O and 90% H_2O/10% D_2O in order to demonstrate direct and relayed through-bond connectivities. The buffer conditions used were the same as those for the TRNOE experiments. [b] Chemical shifts (ppm) are given with respect to 4,4-dimethylsilapentane-1-sulfonate.

The overall B-factor for the complex was 16 $Å^2$, the average B-factor for the hexapeptide 45 $Å^2$, and the average B-factor for the P1 and P1' (nVal-NMeLeu) atoms of the hexapeptide 32 $Å^2$, indicating the higher degree of order or occupancy. The standard deviations from average values were 0.020 Å for 1964 bond lengths and 2.98° for 2716 bond angles. An independent estimate of the upper limits of precision of atomic coordinates, as obtained from a Luzzati plot, is 0.20 Å (Luzzati, 1952).

Further details of the data collection and refinement statistics are given in Table I.

NMR Spectroscopy. ^1H NMR spectra were recorded at 500 MHz on a Bruker AM500 spectrometer equipped with digital phase shifters. Samples for NMR contained 10.5 mM hexapeptide and 0.96 mM PPE (corresponding to a ratio of free to bound ligand of 9.9) in either 99.96% D_2O or 90% H_2O/10% D_2O containing 250 mM KCl, 25 mM potassium phosphate buffer, pH 5.0, and 0.05 mM EDTA. All measurements were carried out at 5 °C, and samples were prepared immediately before use. The pulse sequence for a two-dimensional TRNOE spectrum is identical with that for a conventional NOESY spectrum (Jeener et al., 1979; Macura et al., 1981). The two-dimensional TRNOE spectra were recorded with mixing times of 100 and 150 ms in the pure phase absorption mode by using the time porportional incrementation method (Redfield & Kuntz, 1975; Bodenhausen et al., 1980) as described by Marion and Wüthrich (1983). For the measurements in 90% H_2O/10% D_2O the solvent resonance was suppressed by replacing the last 90° pulse in the NOESY sequence by a 90_x-τ-90_{-x} jump return pulse (Plateau & Gueron, 1982) with the carrier placed at the position of the water resonance and a delay τ of 80 μs. A total of 128 transients was collected for each of 512 increments with a relaxation delay of 1 s between successive transients. The sweep width employed was 7042 Hz with a digital resolution of 6.88 Hz in both dimensions. This was achieved by appropriate zero-filling in the t_1 dimension only. The resonances of the free hexapeptide were assigned from HOHAHA spectra (Davis & Bax, 1985) recorded in D_2O and 90% H_2O/10% D_2O (Table II).

RESULTS

TRNOE Measurements. The theory of the TRNOE method has been discussed in detail previously (Clore & Gronenborn, 1982, 1983), and the technique has been extensively used to study the conformations of ligand bound to macromolecules by both one-dimensional (Gronenborn & Clore, 1982a,b; Gronenborn et al., 1984a,b; Clore et al., 1984, 1986b; Levy et al., 1983) and two-dimensional (Clore et al., 1986a)
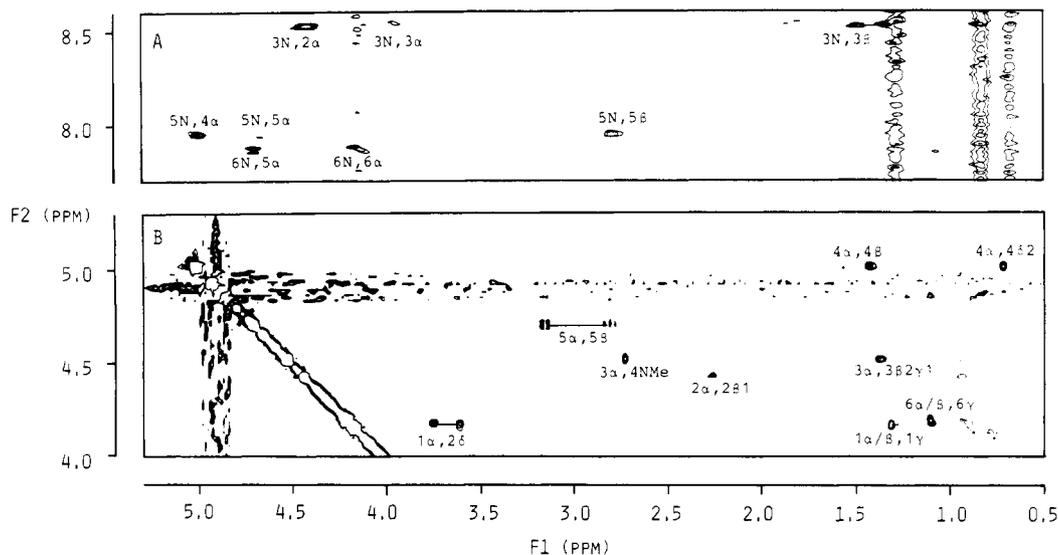
FIGURE 1: (a) NH (F2 axis)–aliphatic (F1 axis) and (b) $C^{\alpha}H/C^{\delta}H$ (F2 axis)–aliphatic (F1 axis) regions of the pure phase absorption 500-MHz two-dimensional TRNOE spectra (mixing time 100 ms) of 10.5 mM hexapeptide and 0.95 mM PPE in (a) 90% H_2O/10% D_2O and (b) 99.96% D_2O buffer containing 250 mM KCl, 25 mM potassium phosphate (pH 5.0), and 0.05 mM EDTA. Inter- and intraresidue TRNOES are labeled.

methods. Consequently, we will only summarize the points relevant to the hexapeptide plus PPE system. The hexapeptide is a small molecule (M_r 706) that lies in the $\omega\tau_c < 1$ regime (where ω is the spectrometer frequency and τ_c the correlation time) such that it exhibits positive NOEs in the free state. Because the values of cross-relaxation rates of the free hexapeptide are very small, no cross-peaks could be observed in NOESY spectra recorded with mixing times of less than 200 ms. (Note that positive NOEs give rise to cross-peaks with sign opposite to that of the diagonal in pure phase absorption NOESY spectra.) The hexapeptide and PPE are in fast exchange on the chemical shift scale so that only a single set of averaged ligand resonances is observed, whose positions are approximately the same as those of the free hexapeptide under the experimental conditions used (viz., a free to bound ratio of ca. 10). The enzyme–ligand complex (M_r ca. 22 000) lies in the $\omega\tau_c \gg 1$ regime such that the cross-relaxation rates of the bound ligand are opposite in sign to those of the free ligand and give rise to negative NOEs. In the presence of excess ligand, NOEs between bound ligand protons are manifested as negative TRNOEs on the averaged ligand resonances and give rise to cross-peaks with the same sign as the diagonal in pure phase absorption NOESY spectra. When all of these factors are taken into account, the magnitude of the negative TRNOE, $N_{ij}(\tau_m)$, at short mixing times τ_m is simply given by the approximation $N_{ij}(\tau_m) \sim (1 - a)\sigma_{ij}^{BB}\tau_m$ in our experiments (where a is the mole fraction of free ligand and σ_{ij}^{BB} the cross-relaxation rate between ligand protons i and j in the bound state).

As the cross-relaxation rates are proportional to $\langle r^{-6} \rangle$, the magnitudes of the TRNOEs provide a sensitive measure of interproton distances between bound ligand protons and hence conformation of the bound ligand. Examples of the NH–aliphatic and $C^{\alpha}H$–aliphatic regions of the 100-ms transferred NOESY spectra are shown in Figure 1. The sequential TRNOEs observed are summarized in Figure 2 and confirm the assignments of the ligand resonances obtained from the HOHAHA spectra. Interresidue TRNOEs were only observed between adjacent residues and were of the type $C^{\alpha}H(i)$–NH(i + 1), $C^{\alpha}H(i)$–proline $C^{\delta}H(i + 1)$, and $C^{\alpha}H(i)$–NMe-LeuNCH$_3$(i + 1). No NH(i)–NH(i + 1), NH(i)–proline $C^{\delta}H(i + 1)$, and NH(i)–NMeLeuNCH$_3$ (i + 1) TRNOEs
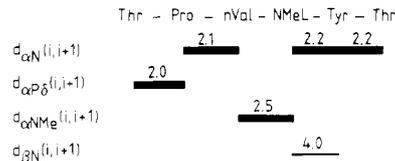

FIGURE 2: Comparison of the observed interresidue TRNOEs (shown as lines) with the corresponding interproton distances derived from the X-ray model. The relative intensity of the TRNOEs is indicated by the thickness of the lines. (Note that within the accuracy of the quantification used, there is no difference in the relative intensities in the 100- and 150-ms mixing time spectra.) As the cross-relaxation rates are proportional to $\langle r^{-6} \rangle$, approximate distance information can be obtained from the relative intensities of the TRNOE cross-peaks by using cross-peaks corresponding to known distances as internal references. On this basis, TRNOEs indicated by the thick and thin lines correspond to distances ≤ 2.5 and ≥ 3.5 Å, respectively. nVal = norvaline; NMeL = N-methylleucine.

were observed. This pattern of TRNOEs is characteristic of an extended backbone conformation (Wüthrich et al., 1984). However, because of the relative paucity of interresidue TRNOEs, as well as the fact that they are limited to immediately adjacent residue, one cannot define the backbone conformation any more precisely. In addition to interresidue TRNOEs, a number of intraresidue TRNOEs was also observed, but these were not sufficiently numerous to define side-chain conformations.

Finally, we note that no evidence of substrate degradation could be detected within the time of the measurements, namely, 24 h at 5 °C. However, after ca. 5 days, signs of substrate degradation could be observed.

X-ray Crystallography. The observation of weak electron density in the difference Fourier maps at the amino and carboxyl termini of the hexapeptide suggests that these portions of the ligand are more flexible in the active site. In contrast, density remained good for the P1 [notation of Schecter and Berger (1967)] nVal backbone and side chain in the primary specificity site. The NMeLeu and Pro residues could be placed in contiguous density at the S1' and S2 subsites, respectively. Residual density at the catalytic Ser-195 and His-57 residues (chymotrypsinogen numbering system) was unambiguous. No contiguous density was found between the Ser-195 O_γ atom and the P1 carbonyl C atom, 3.0 Å (Figure 3); His-57 is in
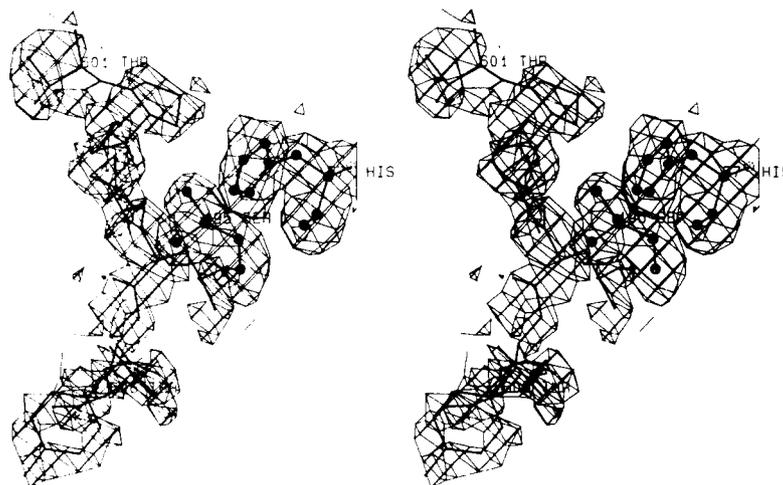
FIGURE 3: Part of the final difference Fourier $(F_o - F_c)$ with a model of the hexapeptide superimposed. The $(F_o - F_c)$ map was obtained with contribution from the hexapeptide to F_c removed. Contouring level is 0.15 e/Å^3. Residues in the hexapeptide are numbered from 601 to 606.

the native conformation, with the $N\epsilon_2$ atom 3.9 Å (nonconstrained) from the N-methyl N atom of the "scissile" bond. While a large residual density is found for the N-methyl N atom and its three neighbors, no marked deviation from planarity could be derived from the shape of the residual density envelope (Figure 3).

The conformation of the bound hexapeptide is extended in nature (see Figure 3) and is fully consistent with the solution TRNOE measurements, as is easily ascertained by a comparison of the interresidue TRNOE intensities with the corresponding interproton distances derived from the X-ray model (see Figure 2).

DISCUSSION

The crystallographic and NMR experiments therefore give every indication of having captured the same relatively long-lived Michaelis complex between a catalytically active enzyme (PPE) and a labile oligopeptide substrate. This is the first time that such a complex has been reported for the serine proteases. The ϕ,ψ backbone torsion angles of the hexapeptide are similar to those of the inhibitor reactive site residues in the complex of human leucocyte elastase and turkey ovomucoid inhibitor third domain (Bode et al., 1986), as well as to similar peptide inhibitor complexes with trypsin (Huber & Bode, 1975), kallikrein (Chen & Bode, 1983), and *Streptomyces griseus* protease B (Read et al., 1984). In the latter cases, the naturally occurring peptide inhibitors, while still extended, have tight, internal cross-linking (disulfide or salt bridges) across the tip of the insertion loop, as discussed by Bode (1986a,b). Here, no loop is possible in an extended chain conformation of the hexapeptide. However, the geometrical constraints imposed by (1) peptide loop cross-linking or (2) scissile N atom methylation suggest a general principle for the mode of action of proteinaceous enzyme inhibitors: conformational flexibility is thus a prerequisite for chain flexing in advancing from (a) trigonal-planar (Michaelis) to (b) tetrahedral-puckered to (c) tetrahedral-N atom inversion states along the microreversible pathway leading to proteolysis. To the extent that the population of one of these states is conformationally hindered, so too would the extent of proteolysis be inhibited.

The assembly of atoms, bonds, and forces employed by nature to make such stable complexes is limited here to the several H-bonds (Table III) and the complementary non-bonded contacts (Table IV), with the significant difference of the methylation of the scissile bond N atom. This methyl group points away from the receptor site of PPE and thus has

Table III: Hydrogen Bond Distances in the Active Site of the PPE-Hexapeptide Complex

hexapeptide	PPE	water molecules	distance (Å)
Thr-601 N	Val-216 O		2.93
Thr-601 $O^{\gamma 1}$		wat-390 OH	2.80
Thr-601 O	Val-216 N		2.52
Pro-602 O	Gln-192 $N^{\epsilon 2}$		3.23
nVal-603 O		wat-408 OH	2.99
nVal-603 O	Gly-193 N		2.64
Tyr-605 N	Thr-41 O		2.87
Tyr-605 $O^{\zeta}H$		wat-411 OH	2.70
Tyr-605 O	Thr-41 $O^{\gamma 1}$		2.62
Thr-606 O		wat-411 OH	3.02

Table IV: Distances Less Than 3.2 Å between Nonbonded Atoms in the Hexapeptide and the Enzyme

hexapeptide	PPE	distance (Å)
Thr-601 $C^{\gamma 2}$	Ser-217 O	3.131
Thr-601 $C^{\gamma 2}$	Arg-2171 N	3.125
Thr-601 $C^{\gamma 2}$	Arg-2171 C^α	2.970
Thr-601 C	Phe-215 C^β	3.179
Thr-601 O	Phe-215 C^α	3.182
Thr-601 O	Val-216 N	2.516
Thr-601 O	Val-216 O	2.953
Pro-602 N	Phe-215 C^β	3.051
Pro-602 C^α	Ser-214 O	2.815
nVal-603 N	Ser-195 O^γ	2.860
nVal-603 C^β	Cys-191 O	3.146
nVal-603 C^δ	Cys-191 O	3.102
nVal-603 C^δ	Thr-213 $C^{\gamma 2}$	3.009
nVal-603 C	Ser-195 O^γ	2.885
nVal-603 O	Gly-193 N	2.640
nVal-603 O	Ser-195 N	3.036
nVal-603 O	Ser-195 C^β	3.110
nVal-603 O	Ser-195 O^γ	2.858
NMeLeu-604 $C^{\delta 1}$	Thr-41 $O^{\gamma 1}$	2.897
NMeLeu-604 $C^{\delta 1}$	Thr-41 O	3.037
NMeLeu-604 $C^{\delta 1}$	Cys-42 S^γ	3.038
Tyr-605 N	Thr-41 O	2.869
Tyr-605 $C^{\delta 2}$	His-40 O	2.818
Tyr-605 O	Thr-41 $O^{\gamma 1}$	2.617

no direct effect on substrate binding. A stereoview of the complex is given in Figure 4.

Due presumably to limitations in the quality of the X-ray data (two crystals measured at 19°, one crystal at 0°), the X-ray experiment is unable to help distinguish among the various intermediate geometries predicted by the Dutler–Bizzozero hypothesis. Further, the TRNOE experiments are
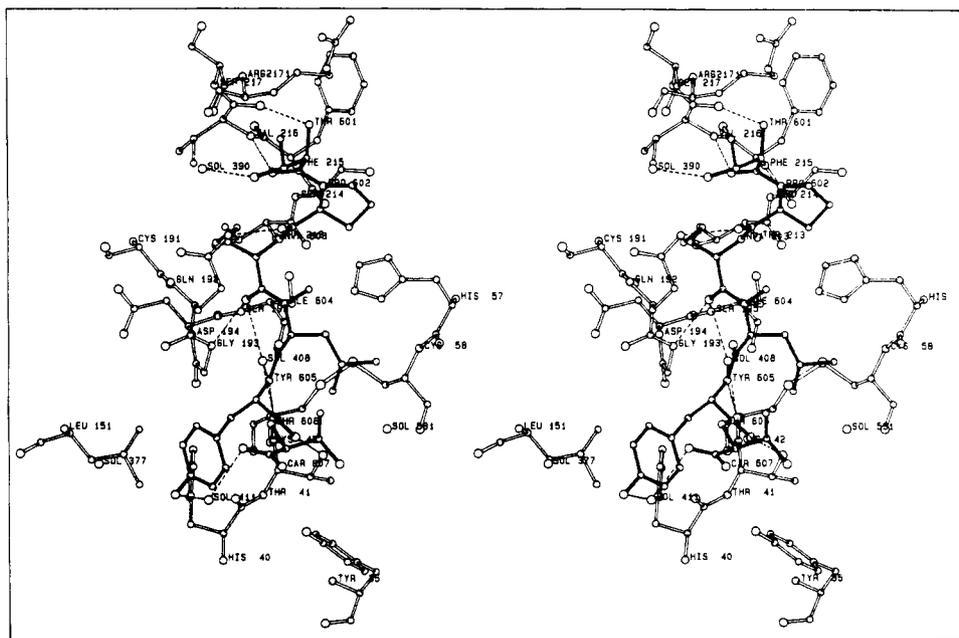
FIGURE 4: Stereoview of the extended active site. Bonds in the hexapeptide are filled. Hydrogen bonds are shown as dashed lines. The S–P interaction region of the extended binding site is above and the S'–P' region below the catalytic Ser–His diad.

unable to help in this matter as they give information only on interproton distances, which solely can be interpreted in terms of a structural model by assuming standard geometry. The possible intermediates are as follows: (1) Ser-195 attack would lead to a pyramidization of the scissile N atom in such a way as to cause the methyl group to point upwards, sterically repelling the concomitant attack of His-57. (2) Stereochemical inversion of this tetrahedral N atom would be required in order to permit attack by His-57. (3) With the scissile N atom in the unfavored geometry, the His-57 role as a proton donor leading to bond cleavage could be usurped by the only other sterically possible source of H atoms, a nearby water molecule. The latter case is an unlikely event, as judged by the tight van der Waals packing of the static model with subsequent exclusion of water. The fluctuations of a dynamically relaxed structure could let such a rare event correspond to the low turnover rate observed from the crystallographic experiment at 19°. (The limited supply of substrate precluded a thorough enzymatic analysis as a function of pH and temperature.)

While individual steps in the microreversible pathway may be exceedingly rapid (e.g., N inversion in ca. 10 ns), the equilibrium structure reported here suggests that the probability of such events which are so facile in "normal" proteolysis is reduced here to a very small value. Both steric and electronic factors must contribute to such a marked change, but these experiments are not able to sort out such differences. In a general way, the equilibrium structure does suggest that the steps must be closely linked in time and concerted in their action, presumably also concerted with receptor-site fluctuations. Specifically, the structure indicates that the Ser O_γ atom attack is not detached from proteolysis during the time frame of the crystallographic experiment.

Both the crystallographic and NMR experiments may therefore best be correlated with a time-averaged structure of an active enzyme and its Michaelis complex. By extending such experiments, designed to bring enzymatic processes within the range of specific physical methods, it may be possible to achieve our objective of illuminating discrete steps along the catalytic pathway, thus augmenting the understanding of the enzymology of the serine proteases as well as aiding in the

design of novel inhibitors and drug design (Powers, 1983).

REFERENCES

Bax, A., & Davis, D. G. (1985) J. Magn. Reson. 65, 355–360.
Bizzozero, S. S., & Zweifel, O. (1975) FEBS Lett. 59, 105–108.
Bizzozero, S. A., & Dutler, H. (1981) Biorg. Chem. 10, 46–62.
Bode, W., Papamakos, E., Musil, D., Seemueller, U., & Fritz, H. (1986a) EMBO J. 5, 813–818.
Bode, W., Wei, A. Z., Huber, R., Meyer, E., Travis, J., & Neuman, S. (1986b) EMBO J. 5, 2453–2458.
Bodenhausen, G., Vold, R. L., & Vold, R. R. (1980) J. Magn. Reson. 37, 93–106.
Chen, Z., & Bode, W. (1983) J. Mol. Biol. 64, 283–311.
Clore, G. M., & Gronenborn, A. M. (1982) J. Magn. Reson. 48, 402–416.
Clore, G. M., & Gronenborn, A. M. (1983) J. Magn. Reson. 65, 355–360.
Clore, G. M., Gronenborn, A. M., & McLaughlin, L. W. (1984) J. Mol. Biol. 187, 119–126.
Clore, G. M., Gronenborn, A. M., Carlson, G., & Meyer, E. F. (1986a) J. Mol. Biol. 190, 259–267.
Clore, G. M., Gronenborn, A. M., Greipl, J. R., & Maass, G. (1986b) J. Mol. Biol. 187, 119–126.
Davis, D. G., & Bax, A. (1985) J. Am. Chem. Soc. 107, 2821–2822.
Deisenhofer, J., Remington, S. J., & Steigemann, W. (1985) Methods Enzymol. 115B, 303–313.
Deslongchamps, P., Chenevret, R., Taillefer, R. J., Moreau, C., & Saunders, J. K. (1975) Can. J. Chem. 53, 1601–1615.
Gronenborn, A. M., & Clore, G. M. (1982a) J. Mol. Biol. 157, 155–160.
Gronenborn, A. M., & Clore, G. M. (1982b) Biochemistry 21, 4040–4048.

Gronenborn, A. M., Clore, G. M., & Jeffrey, J. (1984a) *J. Mol. Biol. 172*, 559–572.

Gronenborn, A. M., Clore, G. M., Brunori, M., Giardina, B., Falcioni, G., & Perutz, M. F. (1984b) *J. Mol. Biol. 178*, 731–742.

Huber, R., Bode, W., Kukla, D., Kohl, W., & Ryan, C. A. (1975) *Biophys. Struct. Mech. 1*, 189–201.

Jack, A., & Levitt, M. (1978) *Acta Crystallogr., Sect. A: Cryst. Phys., Diffr., Theor. Gen. Crystallogr. A34*, 931–935.

Jeener, J., Meier, B. H., Bachman, P., & Ernst, R. R. (1979) *J. Chem. Phys. 71*, 4546–4553.

Levy, H. R., Ejchart, A., & Levy, G. C. (1983) *Biochemistry 22*, 2792–2796.

Luzatti, V. (1952) *Acta Crystallogr. 5*, 802–810.

Macura, S., Huang, Y., Suter, D., & Ernst, R. R. (1981) *J. Magn. Reson. 43*, 259–281.

Marion, D., & Wüthrich, K. (1983) *Biochem. Biophys. Res. Commun. 113*, 967–974.

Meyer, E. F., Radhakrishnan, R., Cole, G. M., & Presta, L. G. (1986) *J. Mol. Biol. 189*, 533–540.

Plateau, G., & Gueron, M. (1982) *J. Am. Chem. Soc. 104*, 7310–7311.

Powers, J. C. (1983) *Annu. Rev. Respir. Dis. 127*, 54–58.

Radhakrishnan, R., Presta, L. G., & Meyer, E. F. (1987) *J. Mol. Biol.* (in press).

Read, R. J., Fuginaga, M., Sielecki, A. R., & James, M. N. G. (1983) *Biochemistry 22*, 4420–4433.

Redfield, A. G., & Kuntz, S. D. (1975) *J. Magn. Reson. 19*, 250–254.

Schecter, I., & Berger, A. (1967) *Biochem. Biophys. Res. Commun. 27*, 157–162.

Schwager, P., Bartels, K., & Jones, T. A. (1977) *J. Appl. Crystallogr. 8*, 275–280.

Steigemann, W. (1974) Ph.D. Thesis, Technical University, Munich.

Swanson, S. M. (1987) *Abstracts of Papers*, Meeting of the American Crystallographic Association, Abstract PB4, American Crystallographic Association, New York.

Wüthrich, K., Billeter, M., & Braun, W. (1984) *J. Mol. Biol. 180*, 715–740.

Crotoxin, a Phospholipase A_2 Neurotoxin from the South American Rattlesnake *Crotalus durissus terrificus*: Purification of Several Isoforms and Comparison of Their Molecular Structure and of Their Biological Activities[†]

Grazyna Faure and Cassian Bon*

Laboratoire des Venins, Unité associée Pasteur/INSERM 285, Institut Pasteur, 28 rue du Dr. Roux, 75015 Paris Cedex 15, France

ABSTRACT: Crotoxin, the major toxin of the venom of the South American rattlesnake *Crotalus durissus terrificus* is a mixture of several isoforms that differ slightly in their molecular structure. The toxin consists of two nonidentical subunits: a basic and weakly toxic phospholipase A_2, component B, and an acidic and nontoxic subunit, component A. In the present investigation, we have used fast-performance liquid chromatography (FPLC) on anionic and cationic exchange columns to purify isoforms of both crotoxin subunits. Two component A isoforms and four component B isoforms were obtained in a homogeneous state, and their purity was verified by isoelectric focusing in polyacrylamide gels. The amino acid composition of the purified component A and component B isoforms was in good agreement with the protein sequences determined previously with mixtures of isoforms. The amino acid compositions indicated that for both crotoxin components the isoforms differed only by the replacement of few amino acid residues. Eight crotoxin complexes have been prepared in a homogeneous state by reassociation of pure component A and component B isoforms. The quantitative comparison of enzymatic and pharmacological properties of the reconstituted crotoxins indicated that the two component A isoforms had identical properties, whereas the four component B isoforms fell in two classes: crotoxin complexes formed with component B isoforms of the first class were enzymatically less active and pharmacologically more potent than those obtained with component B isoforms of the second class.

Crotoxin, the main toxic component of the South American rattlesnake *Crotalus durissus terrificus* was the first animal neurotoxin to be purified and crystallized, half a century ago (Slotta & Fraenkel-Conrat, 1938a). Early investigations also showed that crotoxin possessed a phospholipase activity (Slotta

& Fraenkel-Conrat, 1938b, 1939). Crotoxin exerts its pathophysiological action by blocking neuromuscular transmission (Vital-Brazil & Excell, 1970); its effects are primarily presynaptic, causing a typical triphasic modification of neurotransmitter release from nerve terminals (depression, facilitation, and final blockade) (Hawgood & Smith, 1977; Chang & Lee, 1977; Hawgood & Santana de Sa, 1979). Similar effects are observed with other snake neurotoxins that possess phospholipase A_2 activity, such as β-bungarotoxin (Chang et al., 1973; Strong et al., 1976; Abe et al., 1977), notexin (Harris et al., 1973), taipoxin (Kamenskaya & Thesleff, 1974;